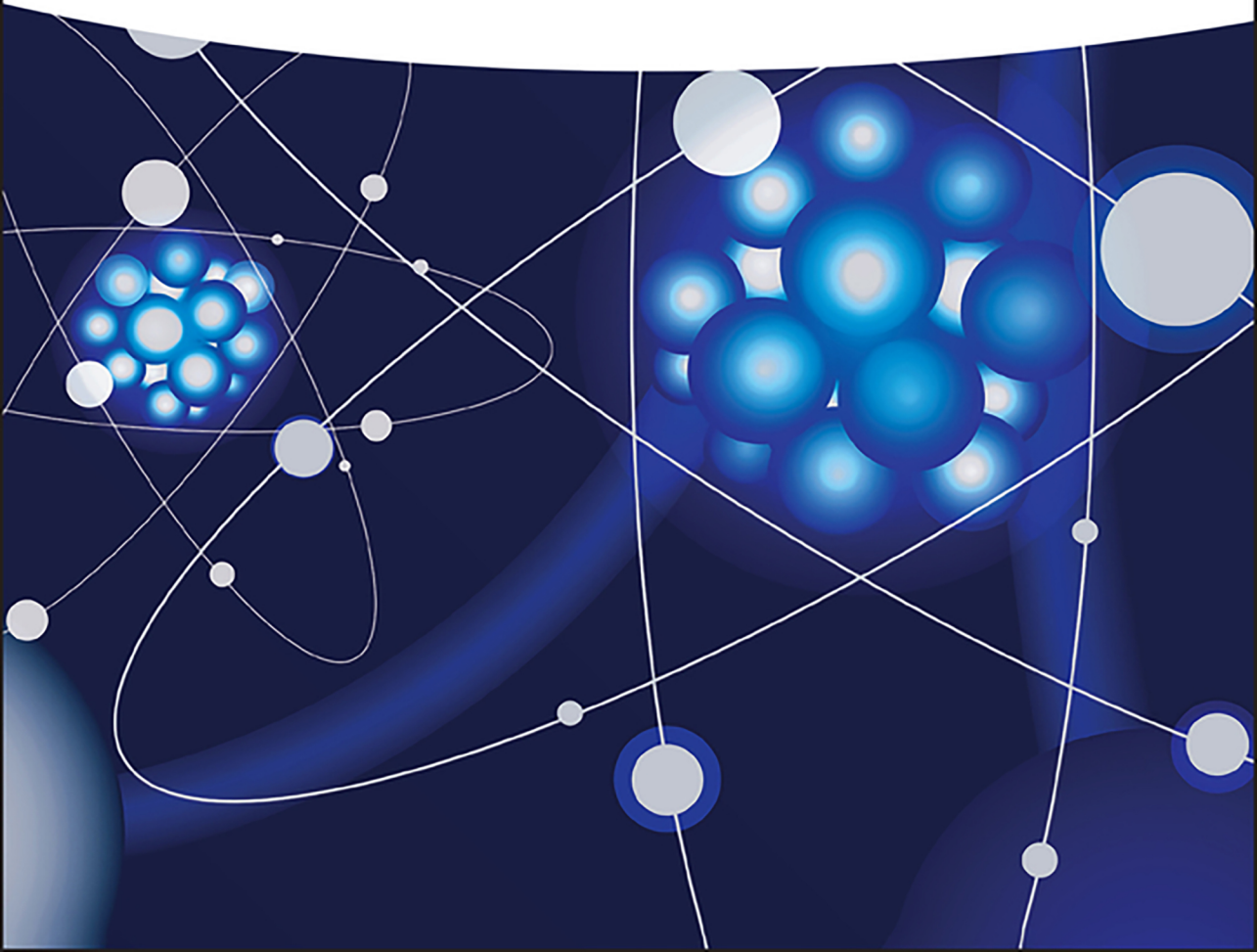


Andrew T.S. Wee, Xinmao Yin, and Chi Sin Tang

# Introduction to Spectroscopic Ellipsometry of Thin Film Materials

Instrumentation, Data Analysis, and Applications





## **Introduction to Spectroscopic Ellipsometry of Thin Film Materials**



# **Introduction to Spectroscopic Ellipsometry of Thin Film Materials**

Instrumentation, Data Analysis, and Applications

*Andrew T. S. Wee*

*Xinmao Yin*

*Chi Sin Tang*

**WILEY-VCH**

## Authors

**Prof. Andrew T. S. Wee**

National University of Singapore  
Department of Physics  
2 Science Drive 3  
Department of Physics  
117542 Singapore  
Singapore

**Prof. Xinmao Yin**

Shanghai University  
Physics Department  
99 Shang Da Road,  
Baoshan District  
200444 Shanghai  
China

**Dr. Chi Sin Tang**

Institute of Materials Research and  
Engineering, Agency for Science,  
Technology and Research (A\*STAR)  
2 Fusionopolis Way  
138634 Singapore  
Singapore

**Cover Image:** © Denis Pobytov/Getty  
Images

All books published by **WILEY-VCH** are carefully produced. Nevertheless, authors, editors, and publisher do not warrant the information contained in these books, including this book, to be free of errors. Readers are advised to keep in mind that statements, data, illustrations, procedural details or other items may inadvertently be inaccurate.

**Library of Congress Card No.:** applied for

**British Library Cataloguing-in-Publication Data:**  
A catalogue record for this book is available  
from the British Library.

**Bibliographic information published by  
the Deutsche Nationalbibliothek**

The Deutsche Nationalbibliothek lists  
this publication in the Deutsche  
Nationalbibliografie; detailed bibliographic  
data are available on the Internet at  
<<http://dnb.d-nb.de>>.

© 2022 WILEY-VCH GmbH, Boschstr. 12,  
69469 Weinheim, Germany

All rights reserved (including those of  
translation into other languages). No part of  
this book may be reproduced in any form – by  
photoprinting, microfilm, or any other  
means – nor transmitted or translated into a  
machine language without written permission  
from the publishers. Registered names,  
trademarks, etc. used in this book, even when  
not specifically marked as such, are not to be  
considered unprotected by law.

**Print ISBN:** 978-3-527-34951-7

**ePDF ISBN:** 978-3-527-83394-8

**ePub ISBN:** 978-3-527-83395-5

**Typesetting** Straive, Chennai, India

Printed on acid-free paper

10 9 8 7 6 5 4 3 2 1

## Contents

### Preface ix

<b>1</b>	<b>Spectroscopic Ellipsometry: Basic Principles</b>	<b>1</b>
1.1	Spectroscopic Ellipsometry	1
1.1.1	p- and s-Polarized Lights and Fresnel Coefficients	2
1.1.2	Representation of Polarized Lights	3
1.2	Principles of Ellipsometric Measurements	5
1.2.1	Rotating-Analyzer Ellipsometer	6
1.3	Experimental Setup	7
1.3.1	VASE Spectroscopic Ellipsometer	8
1.3.2	IR-VASE Spectroscopic Ellipsometer	9
1.4	Spectroscopic Ellipsometry: General Profiles	10
1.5	Ellipsometric Data for Multilayered System	11
1.6	Dielectric Models	12
1.6.1	Drude Model	13
1.6.2	Lorentz Model	14
1.6.3	Drude–Lorentz Model	16
1.6.4	Sellmeier and Cauchy Models	17
1.7	Chapter Summary	18
	References	18
<b>2</b>	<b>Strongly Correlated Systems: Cuprates and Manganites</b>	<b>19</b>
2.1	Introduction	19
2.2	High-Transition-Temperature Superconducting Cuprates	19
2.2.1	The Crystalline Structure of Cuprates	20
2.2.1.1	The Structure of $\text{La}_{1-x}\text{Sr}_x\text{CuO}_4$	20
2.2.1.2	The Structure of $\text{YBa}_2\text{Cu}_3\text{O}_{7-\delta}$	20
2.2.1.3	The Structure of $\text{Nd}_{2-x}\text{Ce}_x\text{CuO}_4$	21
2.2.2	The Electronic Structure of Cuprates	22
2.3	Colossal Magnetoresistance Manganites	26
2.3.1	Crystal Structure of $\text{La}_{1-x}\text{Sr}_x\text{MnO}_3$	26
2.3.2	The Electronic Structure and Magnetism of LSMO	26

2.3.3	Strong and Weak Correlations in Ambipolar Cuprate Thin-Film Systems	28
2.3.4	Samples	29
2.3.5	Spectroscopic Ellipsometry	31
2.4	Charge Localization in Cuprate Thin Film on Oxide Substrate	37
2.5	Plasmon and High-Energy Exciton Excitations in Cuprate Thin Films	40
2.5.1	Observation of the Low- and High-Energy Plasmons in LSCO/STO Film	40
2.5.2	Observation of the High-Energy Excitons in the LSCO/STO Film	43
2.6	Jahn–Teller Splitting Energy Controls the Phase Transition in Manganite Thin-Film Systems	45
	References	49
<b>3</b>	<b>Two-Dimensional Transition Metal Dichalcogenides</b>	<b>59</b>
3.1	Introduction	59
3.2	Crystal Structures of 2D-TMDs	59
3.2.1	1H-Phase	60
3.2.2	1T and 1T'-Phase	61
3.2.3	1H–1T'-Phase Energetics	61
3.2.4	Arising Electronic Structures	61
3.2.4.1	Indirect-to-Direct Bandgap Transition	61
3.2.4.2	Spin–Orbit Splitting	62
3.2.4.3	1T'-Phase Electronic Band Structure	63
3.2.5	2D-TMD: Excitons	64
3.2.5.1	Excitons in 2D-TMDs	65
3.2.5.2	Excitons and Trions	67
3.2.6	Investigative Objectives for 2D-TMDs	67
3.3	Ellipsometry in Probing Structural Phase Transition and Electronic Structures Monolayer-MoS <sub>2</sub>	68
3.3.1	Experimental Results	70
3.3.1.1	Sample Preparation	70
3.3.1.2	Optical Features of Monolayer-MoS <sub>2</sub>	70
3.3.1.3	Inverted and Fundamental Gaps of 1T'-Phase 2D-TMDs	71
3.3.2	Dynamics of 1H–1T'-Phase Transition	72
3.3.2.1	First-Principle Study: Role of Substrates	72
3.3.3	Analyzing the 1H–1T'-Phase Transition of MoS <sub>2</sub> /Cu	75
3.3.3.1	Optical Characterization of MoS <sub>2</sub> /Cu	75
3.3.3.2	Raman and PL Characterization	76
3.3.3.3	Photoemission Spectroscopic Characterization	77
3.3.4	1H–1T'-Phase Transition of WSe <sub>2</sub> /Au	79
3.3.4.1	Optical Characterization of WSe <sub>2</sub> /Au	80
3.3.4.2	Photoluminescence and Photoemission Characterization of WSe <sub>2</sub> /Au	81
3.3.4.3	Phase Transition Yield of 2D-TMDs	84

3.3.5	Section Conclusion	85
3.4	Three-Dimensional Resonant Exciton in Monolayer-WSe <sub>2</sub>	87
3.4.1	Materials, Methods, and Results	88
3.4.1.1	Sample Growth	88
3.4.1.2	Optical Characterization of Monolayer-WSe <sub>2</sub>	89
3.4.1.3	Exciton Peaks: Temperature Dependence	92
3.4.1.4	Fitting Parameters of $\epsilon_2$ Spectra	94
3.4.2	Effects of Temperature on SOC in 2D TMDs	95
3.4.3	High-Energy Photoluminescence Characterization	97
3.4.4	Power-Dependent Photoluminescence Spectroscopic Study	99
3.4.5	Computational Studies	99
3.4.5.1	High-Energy Resonant Exciton Demonstrated via GW-BSE Calculations	99
3.4.5.2	Comparison Between Wannier–Mott and Resonant Excitons	100
3.4.5.3	Origin of Resonant Exciton: Band Structure Calculations Analysis	101
3.4.6	3D-Features of Resonant Exciton in Monolayer-WSe <sub>2</sub> and Thickness Dependence	103
3.4.7	Estimating Exciton Binding Energy	105
3.4.8	Section Summary	105
3.5	Anisotropic Plasmon Excitations in Quasi-Metallic 2D-TMDs	106
3.5.1	Anisotropic Plasmons in 1T'-Phase 2D-TMDs	107
3.5.1.1	Sample Preparation	107
3.5.1.2	Detection of Plasmon in 1T'-Phase WSe <sub>2</sub> /Au	108
3.5.2	One-Dimensional Plasmon in 1T'-Phase WSe <sub>2</sub>	110
3.5.3	Detecting Plasmons in 1T'-Phase MoS <sub>2</sub> /Au Monolayer	112
3.5.4	Analyzing One-Dimensional Plasmon in 1T'-Phase 2D-TMDs	115
3.5.5	1H–1T'-Phase Transition	116
3.5.6	Section Conclusion	117
	References	118
<b>4</b>	<b>Single-Layer Graphene Systems</b>	<b>131</b>
4.1	Introduction	131
4.2	Crystal and Electronic Structure of Graphene	131
4.2.1	Electronic Band Structure of Graphene	132
4.3	Optoelectronic Properties of Graphene	134
4.4	Spectroscopic Ellipsometry Study of Graphene	135
4.4.1	Measurement and Data Analysis of Graphene	135
4.5	Resonant Excitons in Graphene	137
4.6	Substrate-Induced Manipulation of Many-Body Effects	138
4.7	Conclusion and Outlook	141
	References	142
<b>5</b>	<b>Nickelate Systems</b>	<b>149</b>
5.1	Introduction	149
5.2	Crystal Structure	149

5.3	Electronic Structures and Ni3d-Orbital Physics	150
5.4	Phase Diagram and Metal–Insulator Transitions of $\text{RNiO}_3$ Systems	151
5.4.1	Magnetic Phases in $\text{RNiO}_3$ Systems	152
5.5	Optical Characterization via Spectroscopic Ellipsometry	153
5.5.1	Effects of Epitaxial Effects on the Electronic Correlations of Nickelate Thin Films	154
5.5.2	Long-Range Spin Ordering in Nickelate Thin Films	155
5.6	Conclusion and Outlook	159
	References	161
<b>6</b>	<b>Future Development and Applications of Spectroscopic Ellipsometry</b>	<b>167</b>
6.1	Development of Mueller Matrix Imaging Techniques in Spectroscopic Ellipsometry	167
6.2	<i>In Situ</i> Analysis of Langmuir Monolayers	169
6.3	Emergent Properties at Two-Dimensional Interfaces	170
6.4	Micro Devices and Integrated Circuits	171
6.5	Metamaterial Research	172
6.6	Organic Electronics	172
6.7	Biological Materials and Medicines	173
6.8	Anisotropic Materials	173
6.9	Process Control Analysis	173
	References	174
	<b>Index</b>	<b>181</b>

## Preface

Ellipsometry is an experimental technique that boasts of a developmental history spanning more than a century. Initially proposed by Paul Drude in 1887, its first documented use was in 1945. Even though it was then regarded as an unproductive experimental technique, ellipsometry gained traction in the 1990s with advances in computer technology and data processing, necessary for the efficient automation of ellipsometric instrumentation and data analyses. Since then, spectroscopic ellipsometry has established itself as an ultra-sensitive, high-precision optical characterization technique useful in a diverse range of disciplines ranging from semiconductor physics to microelectronics and from biochemistry to real-time characterization of film growth.

Numerous publications have dealt with the fundamentals and analytical techniques of spectroscopic ellipsometry. This book serves as a brief introduction to the ellipsometric technique, and greater emphasis will be devoted to its applications in interfacial properties, electronic structures, and quasiparticle properties of different classes of thin-film materials. This book will focus on two-dimensional transition metal dichalcogenides (2D-TMDs), magnetic oxides such as manganite materials and unconventional superconductors in the form of copper oxide (cuprate) systems. In-depth discussions will be provided on how spectroscopic ellipsometry is utilized to characterize the electronic structures, interfacial properties, and quasiparticle dynamics in novel quantum materials.

Through the in-depth and comprehensive coverage of these materials systems, we demonstrate that spectroscopic ellipsometry remains relevant, and its capabilities continue to advance to cater to the rapidly evolving research landscape. Spectroscopic ellipsometry is therefore a versatile experimental technique for measuring

these unique novel properties. We hope that researchers and graduate students in the field of condensed matter physics and materials science will find this book a useful resource.

*Andrew T. S. Wee*  
National University of Singapore  
Singapore

*Xinmao Yin, PhD*  
Department of Physics, Shanghai University  
China

*Chi Sin Tang*  
Institute of Materials Research and Engineering  
Agency for Science Technology and Research (A\*STAR)  
Singapore

# 1

## Spectroscopic Ellipsometry: Basic Principles

### 1.1 Spectroscopic Ellipsometry

Spectroscopic ellipsometry measures the change of light polarization upon its reflection from the sample. A schematic diagram of the experimental setup is displayed in Figure 1.1. The detector of spectroscopic ellipsometry measures the quantities  $\Psi$  and  $\Delta$  at each corresponding wavelength/photon energy. Parameter  $\Psi$  denotes the ratio of the amplitude of p- to s-polarized reflected light, while  $\Delta$  their phase difference. Specifically, p-polarized light has the electric field vector parallel to the plane of incidence, while s-polarized light consists of the electric field vector perpendicular to the incident plane (Figure 1.2).

Typically, the energy range that is commonly used for spectroscopic ellipsometry measurement is the ultraviolet-visible (UV-vis) regime ( $\sim 0.5\text{--}6\text{ eV}$ ). In this range, sample properties such as the optical band structures and bandgaps can be investigated. Nevertheless, other regions of the electromagnetic spectrum have also been used in spectroscopic ellipsometry measurements. For instance, the use of mid-to-near-infrared range spectroscopic ellipsometry in the study of low-energy structures in  $1T'$ -phase two-dimensional transition metal dichalcogenides (2D-TMDs), such as their fundamental gap and the anisotropic plasmons, will be discussed in Section 3.4 of Chapter 3.

While spectroscopic ellipsometry is a fast, nondestructive, and surface-sensitive (down to a few angstroms) optical characterization technique, the mathematical analysis involved in extracting the optical parameters from the raw ( $\Psi, \Delta$ ) data is not a straightforward process (see Section 1.5 and Figure 1.7). Generally, to analytically elucidate the optical parameters from the raw ( $\Psi, \Delta$ ) data, the sample in consideration must be homogenous, isotropic, and of sufficient thickness. In more general cases, complications will arise and optical models with associated numerical approximation techniques are required for the proper elucidation of meaningful optical results.

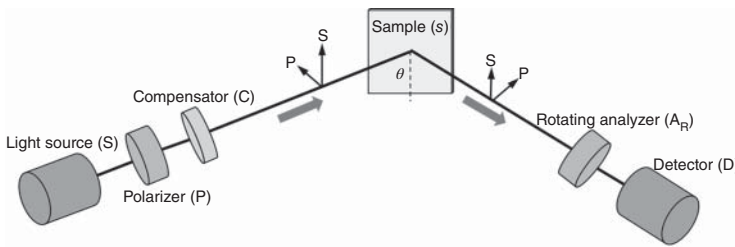


**Figure 1.1** Schematic diagram of spectroscopic ellipsometry with the rotating-analyzer configuration.

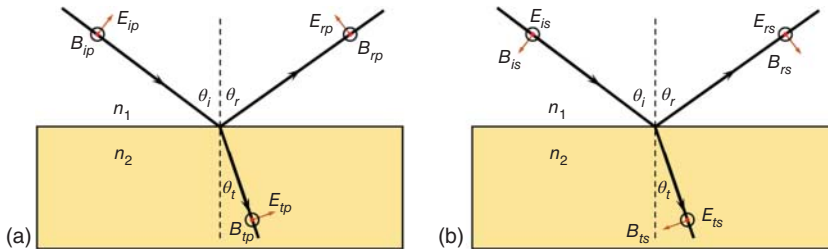


**Figure 1.2** Electric and magnetic fields for (a) p-polarized and (b) s-polarized waves [1].

### 1.1.1 p- and s-Polarized Lights and Fresnel Coefficients

The electromagnetic wave features of light can be expressed in terms of its electric,  $E$ , and magnetic field,  $B$ , components [1]:

$$\vec{E}(\vec{r}, t) = \vec{E}_0 \exp[i(\vec{k} \cdot \vec{r} - \omega t + \delta)] \quad (1.1)$$

$$\vec{B}(\vec{r}, t) = \vec{B}_0 \exp[i(\vec{k} \cdot \vec{r} - \omega t + \delta)] \quad (1.2)$$

where  $\vec{k}$  denotes the wave vector,  $\omega$  denotes the angular frequency, and  $\delta$  denotes the initial phase.

When light is reflected or transmitted through a sample/medium via an oblique angle, the electromagnetic wave can be resolved into two components – p-polarized (in-plane incidence) and s-polarized (perpendicular to incident plane)  $E$ -field components, respectively.

For a medium with refractive index  $n$ , based on Maxwell's equations and boundary conditions, the amplitude of the reflection coefficient for the p-polarized light is expressed as

$$r_p \equiv \frac{E_{rp}}{E_{ip}} = \frac{n_{\{t\}} \cos \theta_i - n_i \cos \theta_t}{n_t \cos \theta_i + n_i \cos \theta_t} \quad (1.3)$$

Likewise, the amplitude of the transmission coefficient for the p-polarized light can be expressed as

$$t_p \equiv \frac{E_{tp}}{E_{ip}} = \frac{2n_i \cos \theta_i}{n_t \cos \theta_i + n_i \cos \theta_t} \quad (1.4)$$

whereas the s-polarized counterparts are expressed as

$$r_s \equiv \frac{E_{rs}}{E_{is}} = \frac{(n_i \cos \theta_i - n_t \cos \theta_t)}{(n_i \cos \theta_i + n_t \cos \theta_t)} \quad (1.5a)$$

$$r_p \equiv \frac{E_{ts}}{E_{is}} = \frac{2n_i \cos \theta_i}{n_i \cos \theta_i + n_t \cos \theta_t} \quad (1.5b)$$

These equations are known as the Fresnel equations. When the refractive indices are complex,  $\tilde{n}$ , the Fresnel equations still hold. The complex dielectric function can be obtained via the expression

$$\tilde{n}^2 \equiv \epsilon \quad (1.6)$$

Based on Snell's law, the Fresnel equations for reflection can be further generalized as

$$r_p = \frac{\tilde{n}_{ti}^2 \cos \theta_i - (\tilde{n}_{ti}^2 - \sin^2 \theta_i)^{\frac{1}{2}}}{\tilde{n}_{ti}^2 \cos \theta_i + (\tilde{n}_{ti}^2 - \sin^2 \theta_i)^{\frac{1}{2}}} \quad (1.7a)$$

$$r_s = \frac{\cos \theta_i - (\tilde{n}_{ti}^2 - \sin^2 \theta_i)^{\frac{1}{2}}}{\cos \theta_i + (\tilde{n}_{ti}^2 - \sin^2 \theta_i)^{\frac{1}{2}}} \quad (1.7b)$$

where  $\tilde{n}$  denotes the complex refractive index and

$$\tilde{n}_{ti} = \frac{\tilde{n}_t}{\tilde{n}_i} \quad (1.8)$$

The reflectances of the p- and s-polarized lights are expressed by

$$R_p \equiv \frac{I_{rp}}{I_{ip}} = \left| \frac{E_{rp}}{E_{ip}} \right|^2 = |r_p|^2 \quad (1.9a)$$

$$R_s \equiv \frac{I_{rs}}{I_{is}} = \left| \frac{E_{rs}}{E_{is}} \right|^2 = |r_s|^2 \quad (1.9b)$$

where the light intensity  $I = n|E|^2$ . Since the difference between  $r_p$  and  $r_s$  is maximized at the Brewster angle [2], ellipsometric measurements are usually performed at incident angles,  $\theta_i$ , typically in the range of 70–80° for the optical characterization of semiconducting systems [3].

In multilayered systems, the resultant amplitude of the reflection coefficients is expressed as the sum of individual components of the reflection and transmission coefficients at each interface. The phase differences of each wave are considered in the analysis.

### 1.1.2 Representation of Polarized Lights

Electromagnetic waves traversing along the  $z$ -direction can be expressed by superimposing two waves that are oscillating parallel to the  $x$ - and  $y$ -axes. The vector sum of the respective  $E$ -fields,  $E_x$  and  $E_y$ , is given by

$$\begin{aligned} E(z, t) &= E_x(z, t) + E_y(z, t) \\ &= E_{x_0} \exp i(\omega t - kz + \delta_x) \hat{x} + E_{y_0} \exp i(\omega t - kz + \delta_y) \hat{y} \end{aligned} \quad (1.10)$$

where  $\hat{x}$  and  $\hat{y}$  denote the unit vectors along the respective axes. Ultimately, the phase difference,  $\delta_y - \delta_x$ , is the most important quantity that determines the state of the polarization of the resultant wave.

To mathematically represent the polarization states and analyze the effects of the optical components in a neat and elegant manner, they are expressed in the form of *Jones vectors* and *Jones matrices* [4].

A complete representation of the polarization of a wave can be expressed in the form of the Jones vector as

$$E(z, t) = \begin{bmatrix} E_{x_0} \exp i\delta_x \\ E_{y_0} \exp i\delta_y \end{bmatrix} \quad (1.11)$$

which can be further simplified as

$$E(z, t) = \begin{bmatrix} E_x \\ E_y \end{bmatrix} \quad (1.12)$$

where  $E_x = E_{x_0} \exp i\delta_x$  and  $E_y = E_{y_0} \exp i\delta_y$ .

Relative changes to the amplitude and phase are important in spectroscopic ellipsometry. Jones vectors are therefore expressed in terms of normalized intensities. Linearly polarized waves along the  $x$ - and  $y$ -axes are expressed, respectively, as

$$E_{\text{lin},x} = \begin{bmatrix} 1 \\ 0 \end{bmatrix} \quad E_{\text{lin},y} = \begin{bmatrix} 0 \\ 1 \end{bmatrix} \quad (1.13)$$

When light is linearly polarized at an orientation of  $45^\circ$ ,

$$E_{+45^\circ} = \frac{1}{\sqrt{2}} \begin{bmatrix} 1 \\ 1 \end{bmatrix} \quad (1.14)$$

In the formalism where optical components are expressed in the form of  $2 \times 2$  matrices, they are known as *Jones matrices*. Based on this formalism, the operation performed on the light by each component in spectroscopic ellipsometry, such as the polarizer, analyzer, and compensator, can be represented as a  $2 \times 2$  matrix operator.

For instance, in the case of a linear polarizer with the azimuthal angle,  $\alpha$ , relative to the  $x$ - $y$  coordinates of a linearly polarized light,  $E_i$ , the process of linear polarization can be expressed as

$$E_f = \begin{bmatrix} \cos \alpha & 0 \\ 0 & \sin \alpha \end{bmatrix} \quad (1.15)$$

Transformations by a series of optical components can be represented by the corresponding series of matrix operations.

While the Jones vector is a concise way for describing polarized light, it is unable to express unpolarized light and light that is partially polarized. Therefore, the *Stokes parameters* (vectors) are used for the description of lights with different polarization [4].

The components of the Stokes vector are

$$\mathbf{S}_0 = I_x + I_y = E_x E_x^* + E_y E_y^* \quad (1.16a)$$

$$\mathbf{S}_1 = I_x - I_y = E_x E_x^* - E_y E_y^* \quad (1.16b)$$

$$\mathbf{S}_2 = I_{+45^\circ} + I_{-45^\circ} = 2E_{x_0} E_{y_0} \cos \Delta \quad (1.16c)$$

$$\mathbf{S}_3 = I_R - I_L = -2E_{x_0} E_{y_0} \sin \Delta \quad (1.16d)$$

where  $I_x$  and  $I_y$  denote the intensities of the linearly polarization light along the  $x$ - and  $y$ -axes, respectively. Likewise,  $I_{\pm 45^\circ}$  represents light polarization  $\pm 45^\circ$  to the  $x$ -axis, while  $I_L/I_R$  represent intensities of left-/right-circularly polarized light. Finally,  $\Delta = \delta_x - \delta_y$ .

The Stokes vector can also be expressed as

$$\mathbf{S} = \begin{bmatrix} \mathbf{S}_0 \\ \mathbf{S}_1 \\ \mathbf{S}_2 \\ \mathbf{S}_3 \end{bmatrix} \quad (1.17)$$

Transformation of a Stokes vector can be expressed via a  $4 \times 4$  matrix representation, also known as a *Mueller matrix*. The calculation is performed in a fashion similar to the Jones matrix. For instance, when linear polarization oriented at  $45^\circ$  passes a polarizer with transmission axis along the  $x$ -direction, the resultant light that emerges from the polarizer is transformed via the following:

$$\frac{1}{2} \begin{pmatrix} 1 & 1 & 0 & 0 \\ 1 & 1 & 0 & 0 \\ 0 & 0 & 0 & 0 \\ 0 & 0 & 0 & 0 \end{pmatrix} \begin{pmatrix} 1 \\ 0 \\ 1 \\ 0 \end{pmatrix} = \begin{pmatrix} 1/2 \\ 1/2 \\ 0 \\ 0 \end{pmatrix} \quad (1.18)$$

## 1.2 Principles of Ellipsometric Measurements

When light is reflected/transmitted from a sample, the p- and s-polarized components of the incident light undergo changes to their amplitude and phase. Hence, spectroscopic ellipsometry is a technique that capitalizes on these changes where the essential optical parameters are derived. As mentioned, the raw quantities measured using ellipsometry are  $\Psi$  and  $\Delta$ , representing the amplitude ratio and phase difference between reflected or transmitted p- and s-polarized waves, respectively. These two quantities are related complex reflection coefficients via the expression

$$\rho \equiv \tan \Psi \exp i\Delta = \frac{r_p}{r_s} \quad (1.19)$$

with  $r_p$  and  $r_s$  defined as ratios of the light reflected to the incident  $E$ -fields.

Equation (1.19) can be further expressed as

$$\tan \Psi \exp i\Delta = \frac{r_p}{r_s} = \frac{E_{rp}/E_{ip}}{E_{rs}/E_{is}} = E_{rp}/E_{rs} \quad (1.20)$$

where the final step of simplification can be performed since  $E_{ip} = E_{is}$ .

Different spectroscopic ellipsometry setups are available, of which the raw  $\Psi$  and  $\Delta$  are measured by different means. Generally, the systems are classified into two main categories – spectroscopic ellipsometers with rotating optical elements and those with photoelastic modulators. In our study, focus will be on the system with rotating optical elements (i.e. rotating analyzer with compensator). The working principle of such spectroscopic ellipsometers will be described briefly in Section 1.2.1.

### 1.2.1 Rotating-Analyzer Ellipsometer

A rotating-analyzer spectroscopic ellipsometer (Figure 1.1) is one of the few ellipsometric setups that is widely used. The changes made to an incident light wave when passing through a rotating-analyzer spectroscopic ellipsometer can be represented as a series of matrix operations  $PSA_R$ , where  $P$ ,  $S$ , and  $A_R$  denote the polarizer, the sample, and the rotating analyzer, respectively. In spectroscopic ellipsometry, the wavelength of the incident photon is typically changed using a monochromator. However, this slows down the operational speed of the system. Hence, in many spectroscopic ellipsometry systems, especially those for real-time monitoring, a grating spectrometer is typically used in the detector probe, while white light is used as the incident source.

By applying the Jones vectors and Mueller matrices, the output of the  $PSA_R$  ellipsometric configuration can be expressed as

$$L_{\text{out}} = AR(A)R(-P)PL_{\text{in}} \quad (1.21)$$

where the Jones vector of the light wave at the detector can be expressed as  $L_{\text{out}} = \begin{bmatrix} E_A \\ 0 \end{bmatrix}$ .  $L_{\text{in}} = \begin{bmatrix} 1 \\ 0 \end{bmatrix}$  denotes the input Jones vector of the incident light source.  $R(A)$  represents the rotation matrix with a rotation angle of the analyzer at  $A$ .  $P$  denotes the rotation angle of the polarizer and  $S$  represents the Jones matrix corresponding to the reflected light off the sample.

Hence, Eq. (1.21) is expressed in the matrix form as

$$\begin{bmatrix} E_A \\ 0 \end{bmatrix} = \begin{bmatrix} 1 & 0 \\ 0 & 0 \end{bmatrix} \begin{bmatrix} \cos A & \sin A \\ -\sin A & \cos A \end{bmatrix} \begin{bmatrix} \sin \Psi \exp i\Delta & 0 \\ 0 & \cos \Psi \end{bmatrix} \begin{bmatrix} \cos P & -\sin P \\ \sin P & \cos P \end{bmatrix} \begin{bmatrix} 1 & 0 \\ 0 & 0 \end{bmatrix} \begin{bmatrix} 1 \\ 0 \end{bmatrix}$$

If polarization angle  $P = 45^\circ$ , it will then take the form

$$\begin{bmatrix} E_A \\ 0 \end{bmatrix} = \begin{bmatrix} 1 & 0 \\ 0 & 0 \end{bmatrix} \begin{bmatrix} \cos A & \sin A \\ -\sin A & \cos A \end{bmatrix} \begin{bmatrix} \sin \Psi \exp i\Delta \\ \cos \Psi \end{bmatrix} \quad (1.22)$$

which ultimately leads to the solution

$$E_A = \cos A \sin \Psi \exp i\Delta + \sin A \cos \Psi \quad (1.23)$$

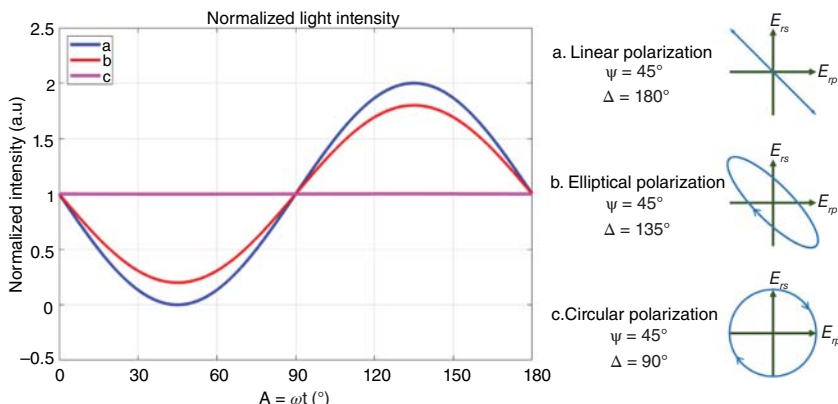


**Figure 1.3** Normalized intensity of linearly, elliptical, and circularly polarized light based on the rotating-analyzer configuration.

The light intensity registered at the detector can then be expressed as the modulus square of  $E_A$ :

$$\begin{aligned}
 I &= |E_A|^2 \\
 &= I_0(1 - \cos 2\Psi \cos 2A + \sin 2\Psi \cos \Delta \sin 2A) \\
 &= I_0(1 + S_1 \cos 2A + S_2 \sin 2A)
 \end{aligned} \tag{1.24}$$

where  $I_0$  represents the proportionality constant of the reflected light. The period of the intensity variation is  $\pi$  radians ( $180^\circ$ ). Generally, the Stokes parameters,  $S_1$  and  $S_2$ , in a rotating-analyzer ellipsometer (RAE) are measured as Fourier coefficients of  $\cos 2A$  and  $\sin 2A$ , respectively. When the analyzer rotates at an angular frequency of  $\omega$ , the general expression of the detector intensity is expressed as

$$I(t) = I_0(1 + \alpha \cos 2\omega t + \beta \sin 2\omega t) \tag{1.25}$$

where the normalized intensity registered at the detector based on Eq. (1.25) is plotted in Figure 1.3.

## 1.3 Experimental Setup

The spot size of the beam is in the range of 3–5 mm with additional detachable microfocus, which can be used to focus the spot size to an even smaller dimension of about 200  $\mu\text{m}$ . Such a small beam spot is suitable for the optical characterization of smaller samples to reduce the instances of back reflection and scattering in transparent samples.

The input unit consists of a lens mount, a polarizer stage, and an alignment detector socket. Polarization state of the light beam is detected before its incidence on the sample, which is mounted on the sample stage. After reflecting off the sample surface, the detector unit converts the reflected beam into a voltage and measures

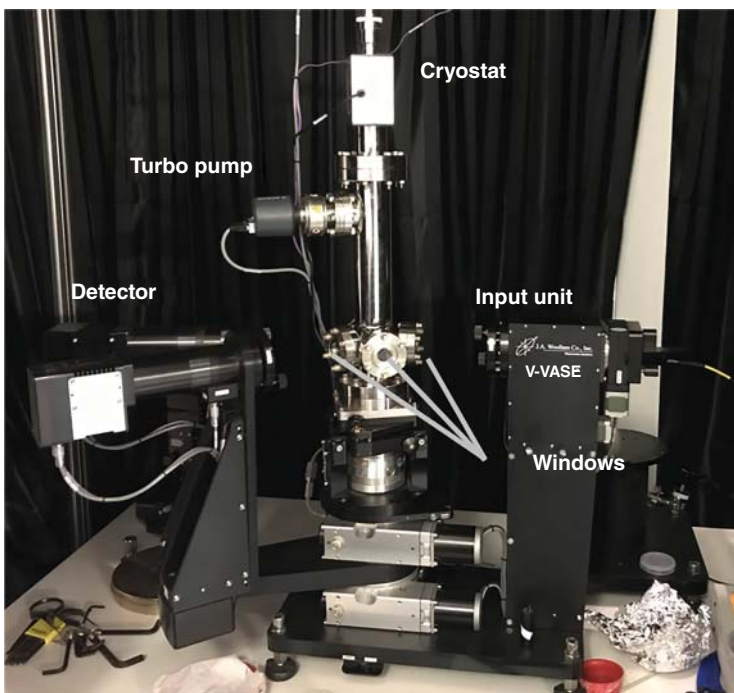


**Figure 1.4** Woollam VASE spectroscopic ellipsometer.

its polarization state. The software (WVASE32) is then used to analyze the raw data from which the optical parameters of the sample are derived.

### 1.3.1 VASE Spectroscopic Ellipsometer

The setup of the Variable-Angle Spectroscopic Ellipsometer (VASE) by J. A. Woollam Co., Inc. is displayed in Figure 1.4. The arc lamp provides a broadband light source for the HS-190 monochromator (Czerny-Turner Scanning Monochromator), which the software uses to supply a selected wavelength/photon energy of light for the system. This spectroscopic ellipsometer provides both high accuracy and precision along with a wide spectral range of  $\sim 190\text{--}2500\text{ nm}$  ( $\sim 0.5\text{--}6.5\text{ eV}$ ), covering the near-IR, visible, and near-UV regimes. With this broad spectral range, this system is suitable for characterizing optical bandgaps and electronic transitions for semiconducting and Mott-insulating systems (Figure 1.5).

RAE of the VASE spectroscopic ellipsometer helps to maximize data accuracy near the “Brewster” angle [1], where the raw  $\Psi$  and  $\Delta$  data are content-rich. The autot retarder is a computer-controlled waveplate that modifies the beam polarization (from linear to circular polarization or vice versa) before reaching the sample. This process provides greater accuracy for the measurement of the  $\Delta$  parameter even when the phase difference is close to the extremum angles of  $0^\circ$  and  $180^\circ$ . This process produces optimum measurement conditions for the sample.